Photochemistry and Photobiology, 2019, 95: 1160–1168

Alkane Chain-extended Pterin Through a Pendent Carboxylic Acid Acts as Triple Functioning Fluorophore, $^1O_2$ Sensitizer and Membrane Binder

Niluksha Walalawela[1,2], María Noel Urrutia[3], Andrés H. Thomas[3], Alexander Greer*[1,2] and Mariana Vignoni*[3]

[1]Department of Chemistry, Brooklyn College, City University of New York, Brooklyn, NY
[2]Ph.D. Program in Chemistry, The Graduate Center of the City University of New York, New York, NY
[3]Instituto de Investigaciones Fisicoquímicas Teóricas y Aplicadas (INIFTA), Departamento de Química, Facultad de Ciencias Exactas, Universidad Nacional de La Plata (UNLP), CCT La Plata-CONICET, La Plata, Argentina

Received 4 February 2019, accepted 12 March 2019, DOI: 10.1111/php.13098

ABSTRACT

In order to develop a new long alkane chain pterin that leaves the pterin core largely unperturbed, we synthesized and photochemically characterized decyl pterin-6-carboxyl ester (CapC) that preserves the pterin amide group. CapC contains a decyl-chain at the carboxylic acid position and a condensed DMF molecule at the N2 position. Occupation of the long alkane chain on the pendent carboxylic acid group retains the acid–base equilibrium of the pterin headgroup due to its somewhat remote location. This new CapC compound has relatively high fluorescence emission and singlet oxygen quantum yields attributed to the lack of through-bond interaction between the long alkane chain and the pterin headgroup. The calculated lipophilicity is higher for CapC compared to parent pterin and pterin-6-carboxylic acid (Cap) and comparable to previously reported *O*- and *N*-decyl-pterin derivatives. CapC's binding constant K_b (8000 M^{-1} in *L*-α-phosphatidylcholine from egg yolk) and Φ_F:Φ_Δ ratio (0.26:0.40) point to a unique triple function compound, although the hydrolytic stability of CapC is modest due to its ester conjugation. CapC is capable of the general triple action not only as a membrane intercalator, but also fluorophore and $^1O_2$ sensitizer, leading to a "self-monitoring" membrane fluorescent probe *and* a membrane photodamaging agent.

INTRODUCTION

Pterins comprise a family of naturally occurring heterocyclic compounds derived from 2-aminopteridin-4(*1H*)-one. Pterins can be found in many biological systems playing various roles such as pigments in insects, and enzymatic cofactors for redox and one-carbon transfer reactions (1,2). Under UVA excitation (320–400 nm), pterins can fluoresce, undergo photo-oxidation and generate reactive oxygen species (ROS) (3,4). In the presence of oxygen, pterins are involved in both Type I and Type II photosensitized oxidation reactions (5), inducing DNA damage and the photoinactivation of enzymes and bacteria (6–8). In addition, natural pterins are able to photo-oxidatively damage membranes although not through intercalation, as they readily passed through membranes (9). In view of this last point, we have been interested in creating pterins for better photo-oxidation control within membranes.

Interestingly, native pterins are also difficult to solubilize. They have sparing solubility in water and are almost insoluble in organic solvents, which has been a drawback in pterin research. In order to help solve these solubility problems and their general lack for membrane intercalation, we recently reported on a decyl-chain alkylation reaction to reach *O*- and *N*-decyl-pterins **1**–**4**, as shown in Fig. 1. The *O*- and *N*-sites refer to the *O4*- and *N3*-positions where the decyl-chain added to the pterin. Here, the origins in the alkylation reactions were determined *O*- and *N*-sites with a kinetic preference for the former (10,11). Such *O*- and *N*-alkylation led to increased organic solvent solubility and enabled membrane binding, but perturbed the pterin core by removing its natural acid–base equilibrium (Fig. 1). The applicability of the long alkane chain attachment to membrane binding seemed clear to us. Long alkyl chains in such compounds are flexible, and chain folding can also occur due to its high conformational freedom. It is known that alkane chains can coil back via *gauche* interactions at the expense of all-*trans* interactions (12). However, most importantly, chain alkylation of pterin facilitated their intercalation in large unilamellar vesicles (LUVs). Of particular interest was that a decyl-chain pterin not only efficiently peroxidized lipids, but that phospholipid of the membranes were also chain-shortened thereby highly destabilizing the LUVs (13). But membrane-binding functionality is just one of three other facets on our mind for pterins.

Over the past 6–8 years, "smart" compounds that possess dual fluorescence sensing and singlet oxygen sensitizing properties have become a hot topic (14–16), with success reported in dual function image-guided and photodynamic therapy applications (PDT) (17–25). Indeed, our previous *O*- and *N*-decyl-pterins possessed good singlet oxygen quantum yields (Φ_Δ), but had poor fluorescence quantum yields (Φ_F) some 4–30 fold less compared to native pterin, thereby fulfilling only two of three facets, even though a minor fluorescence increase was observed when intercalated in the membrane (10). As a result, we surmised that the low Φ_F was related to the position of the alkylation, as the chain is attached to the aromatic ring, significantly reducing their capacity as fluorescent imaging probes in lipid membranes.

*Corresponding authors' emails: agreer@brooklyn.cuny.edu (Alexander Greer) and mvignoni@inifta.unlp.edu.ar (Mariana Vignoni)

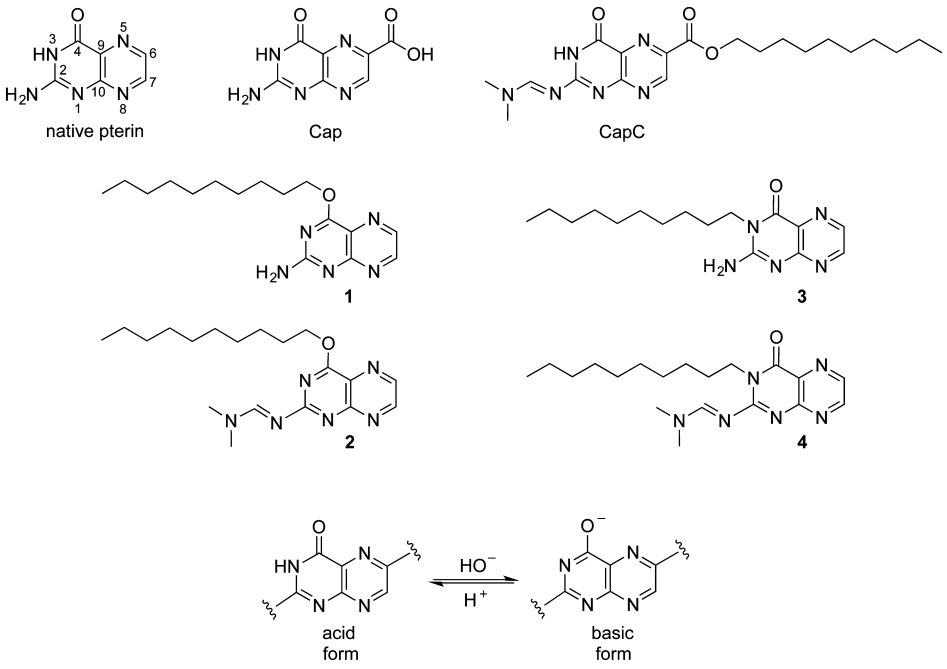

Figure 1. Structure of native pterin with general numbering scheme, pterin-6-carboxylic acid (Cap), decyl pterin-6-carboxylate (CapC), *O*-decyl-pterin **1**, biguanide-like *O*-decyl-pterin **2**, *N*-decyl-pterin **3** and biguanide-like *N*-decyl-pterin **4**. Acid–base forms of native pterin, Cap and CapC, but unavailable in the *O*- and *N*-decyl-pterins **1**–**4**.

Therefore, we have begun to explore pterin-6-carboxylic acid (Cap) as a starting reactant, which provides a carboxyl handle to attach the alkyl chain presumably without significantly affecting structure of aromatic heterocyclic ring. The new compound obtained, CapC, contains a condensed DMF molecule, which is structurally similar to biguanide compounds bearing R_2N-C(NH)-NH-C(NH)-NH_2 groups used for the treatment of cancer and for immunosuppression (26–29).

To our knowledge, no previous synthesis has been reported for functionalizing the pendant carboxylic acid group of Cap. Thus, we report on CapC's (i) synthesis and characterization, (ii) fluorescence and $^1O_2$ quantum yields and (iii) computed solubility and membrane binding. The synthetic reaction to form a covalent bond to the carboxylic acid group of Cap is new. CapC is also the only pterin compound yet known for trimodal functionality. Trimodal functionality is intended to mean a triple function for favorable membrane intercalation as well as fluorescence emission and singlet oxygen production, which is elucidated below.

MATERIALS AND METHODS

Chemicals. Pterin-6-carboxylic acid (Cap), 1-iododecane, potassium carbonate (K_2CO_3), sodium chloride (NaCl), sodium sulfate (Na_2SO_4), *N, N*-dimethylformamide (DMF), dichloromethane (DCM), deuterated dimethyl sulfoxide (DMSO-d_6, 99.5%) and L-α-phosphatidylcholine from egg yolk (eggPC) were obtained from Sigma and used as received. Tris (hydroxy-methyl)aminomethane (Tris) was provided by Genbiotech. Chloroform was from U.V.E., and acetonitrile and methanol were from J. T. Baker, HPLC grade. Water was purified with a deionization system.

Synthesis of decyl(E)-2-(((dimethylamino)methylene)amino)-4-oxo-3,4-dihydropteridine-6-carboxylate (CapC). Potassium carbonate (7 mg, 0.05 mmol) was added to a solution of Cap (10 mg, 0.05 mmol) in DMF (12 mL). The mixture was sonicated and sparged with argon for 20 min. Then, 1-iododecane (50 μL, 0.25 mmol) was added to the solution. The reaction mixture was placed in an oil bath and stirred at 95°C for 48 h. The solution was cooled to room temperature, and the solvent was evaporated to dryness under vacuum providing a solid residue. This solid residue was treated with NaCl (s.s.) (40 mL) and then extracted with DCM (3 × 50 mL). The organic layers were separated, dried over Na_2SO_4, filtered and evaporated to dryness. The crude residue obtained was purified by silica gel column chromatography to obtain 96% pure product (eluent: DCM 100% was followed by 100→95% DCM/methanol mixtures). The product was further purified to obtain 99% pure product using a Shimadzu HPLC apparatus with PDA detector equipped with a Synergi Polar-RP column (ether-linked phenyl phase with polar end-capping, 150 × 4.6 mm, 4 μm, Phenomenex) for product separation. The mobile phase was methanol, and the runs were carried out with a flow of 0.3 mL min^{-1}. The compound was stored in solid state, at 4°C and in the dark. Yield: 8 mg (44%), purity 96%. R_f (methanol/DCM, 5:95 v/v): 0.48; t_R HPLC = 10.3 min. ^{1}H NMR (400 MHz, DMSO-d_6): δ 12.22 (s, 1H), 9.20 (s, 1H), 8.89 (s, 1H), 4.34 (t, J = 7 Hz, 2H), 3.26 (s, 3H), 3.13 (s, 3H) 1.75 (m, 2H), 1.30–1.51 (m, 14H), 0.84 (t, J = 7 Hz, 3H). ^{13}C NMR (100.6 MHz, DMSO-d_6): δ 163.4(C), 161.3(C), 159.8(C–H), 159.8(C), 157.9(C), 150.2(C–H), 137.2 (C), 130.5(C), 65.3, 41.2, 35.2, 31.3, 28.9, 28.9, 28.8, 28.7, 28.5, 25.8, 22.1, 14.0. HRMS (ESI): *m/z* calcd for $C_{20}H_{31}N_6O_3$ [M + H^+] = 403.2452, found 403.2460.

Absorption measurements. Absorption spectra were recorded on a Shimadzu UV-1800 spectrophotometer, using quartz cells of 0.4 or 1 cm optical path length.

Nuclear magnetic resonance. ^{1}H, ^{13}C, ^{13}C-APT and 2D NMR spectra were recorded on a Bruker 400 MHz NMR spectrometer. ^{13}C-APT NMR was carried out based on the technique described elsewhere (30).

Mass spectrometry. The liquid chromatography equipment/mass spectrometry (LCMS) system was equipped with an UPLC chromatograph (ACQUITY UPLC from Waters) coupled to a quadrupole time-of-flight mass spectrometer (Xevo G2-QTof-MS from Waters) (UPLC-QTof-MS). UPLC analyses were performed using an Acquity UPLC BEH Shield RP18 column (1.7 μm; 2.1 × 100 mm) (Waters) and gradient elution starting with 40% water and 60% of acetonitrile and finishing with 80% acetonitrile, at a flow rate of 0.2 mL min^{-1}. The mass spectrometer was operated in positive mode with a capillary voltage of 2.5 kV, the cone voltage of 30 V, the cone gas flow of 20 L h^{-1}, the source temperature set to 130°C and the desolvation temperature set to 450°C.

Fluorescence measurements. Steady-state and time-resolved fluorescence measurements were performed at room temperature using a single-photon-counting equipment FL3TCSPC-SP (Horiba Jobin Yvon), described elsewhere (31). The fluorescence quantum yields (Φ_F) were determined from the corrected fluorescence spectra using equation 1:

$$\Phi_F = \Phi_F{}^R I A^R / I^R A \quad (1)$$

where I is the integrated intensity, A is the absorbance at the excitation wavelength (λ_{exc}) and the superscript R refers to the reference fluorophore. In our experiments, quinine bisulfate (Riedel-de Haën, Seelze, Germany) in 0.5 M H_2SO_4 (Φ_F = 0.546) (32) was used as a reference. To avoid inner filter effects, the absorbance of the solutions, at the excitation wavelength, was kept below 0.10. Spectra were corrected for wavelength-dependent emission profiles with corrections factors supplied by the manufacturer and using the software FluorEssence™ version 2.1 (Horiba Jobin Yvon).

Singlet oxygen measurements. For $^1O_2$ detection, the experiments were carried out at room temperature using acetonitrile as a solvent since the lifetime of $^1O_2$ (τ_Δ) is long enough to detect it (33). The $^1O_2$ emission in the near-infrared (NIR) region was registered using a NIR PMT Module H10330-45 (Hamamatsu) coupled to the equipment FL3 TCSPC-SP mentioned above, as described elsewhere (34). Corrected emission spectra obtained by excitation at 366 nm were recorded between 950 and 1400 nm, and the total integrated $^1O_2$ phosphorescence intensities (IP) were calculated by integration of the emission band centered at ca. 1270 nm. Quantum yields of $^1O_2$ production (Φ_Δ) were determined as described in Ref. 10.

Computed partition coefficient. Octanol to water partitioning log P was calculated with the MarvinSketch 17.1.2 (ChemAxon Ltd. Budapest, Hungary). Based on literature (35,36), the accuracy of the computed log P values is approximately ± 0.8.

Steady-state irradiation. Photolysis of compound CapC in different solvents was carried out irradiating in quartz cells (0.4 cm optical path length). One Rayonet RPR 3500 lamp (Southern New England Ultraviolet Co.) with emission centered at 350 nm [band width (fwhm) 20 nm] was employed as radiation source. The irradiance was 13 ± 1 W m^{-2}, calculated after measuring the incident photon flux density using Aberchrome 540 (Aberchromics Ltd.) as an actinometer (37).

Preparation of LUVs. EggPC was dissolved in chloroform and dried under nitrogen stream to generate LUVs. LUVs were formed by hydrating in Tris buffer (20 mM, pH 7.4). The samples were vortexed for a few minutes, followed by extrusion through a 100 nm porous membrane (Avanti Polar). LUVs were kept at 4°C prior used.

LUV binding constants. A titration method (38) was used to determine the binding constant (K_b). To a solution of the corresponding pterin derivative in buffer TRIS, gradually increasing quantities of eggPC LUVs were added. The mixture was shaken and incubated for ~15 min, and the fluorescence spectrum was recorded. Kinetic experiments were performed to ensure equilibrium conditions. Corrected fluorescence spectra obtained by excitation at 360 nm were recorded between 390 and 600 nm, and the total fluorescence intensities (F) were calculated by integration of the fluorescence band between 410 and 600 nm. This parameter was then plotted on a graph against the lipid concentration, and equation 2 was used to fit the data:

$$F_L = F_0 + (F_\infty - F_0) \times [L]/(1/K_b + [L]) \quad (2)$$

where the three values F_0, F_L and F_∞ are the fluorescence intensity of the compound without lipid, with lipid at concentration L, and that which would be obtained asymptotically at complete binding, respectively, and [L] is eggPC concentration.

RESULTS AND DISCUSSION

Regioselective synthesis of CapC

A mildly basic reaction condition (K_2CO_3) was used for the decyl-chain alkylation of Cap in *N,N*-dimethylformamide (DMF) at 95°C (Scheme 1). CapC was obtained as the major product in 44% yield along with other uncharacterized by-products. Cap has two ionizable protons, one at the carboxylic acid site (pK_{a1} = 3.1) and the other on the pterin amide group (pK_{a2} = 7.9) (3). The low pK_{a1} of Cap led to carboxylate anion formation for regioselective alkylation of iododecane at the carboxyl site. LCMS data suggested that CapC contained a single decyl-chain and a condensed DMF molecule (MS calcd for $C_{20}H_{31}N_6O_3$ [M + H^+] = 403.2452, found 403.2460) (Fig. S4).

Evidence for the structural assignment of CapC was acquired with ^1H and ^{13}C NMR. Interestingly, the ^{13}C spectrum showed only seven aromatic signals, even though the compound has eight carbons that should appear in the aromatic region (100–200 ppm). Therefore, a ^{13}C-APT NMR experiment was carried out to resolve possible peak overlaps (30). Figure 2a shows the expanded portion of ^{13}C and ^{13}C-APT resolving the peaks closely residing at 159.87 ppm (negative) and 159.85 ppm (positive), corresponding to C–H and quaternary C, respectively.

Further structural evidence for the decyl-chain connection to Cap was obtained with HMBC spectroscopy. Figure 2b shows the expanded HMBC spectrum and the relationship between O–CH_2 peak (4.34 ppm) and the aromatic carbons. The HMBC spectrum shows a single cross-peak, which suggests an exocyclic connection and rules out endocyclic connections (N1, N5, N8), leaving only a possible connection at "g" (N3 connection is not possible because a DMF molecule is condensed at that position). Elaborating on the DMF condensation, Scheme 2 shows our proposed mechanism for the formation of biguanide-like portion of CapC from the condensation of a DMF molecule. Overall, the NMR and mass spectrometry evidence indicates that the decyl-chain is attached to the carboxylic acid group of Cap and a DMF molecule is condensed at the N2 position.

Absorption, fluorescence and $^1O_2$ generating properties of CapC

CapC was dissolved in methanol/water 1:3 (*v/v*), and the absorption spectra were recorded at two different pH values, 4 and 11. Different spectra were detected for each pH (Fig. 3), thus revealing pterin acid–base forms. The basic form has a higher energy band blueshifted compared to the acid form (300 and 320 nm, respectively), while a lower energy band is redshifted compared to the acid form (376 and 360 nm, respectively) (Fig. 3). This spectral shifting pattern is typical of the aromatic water-soluble pterins (3) and was not observed for *O*- and *N*-decyl-pterins **1**–**4** (10), since the alkylation to the amide group eliminated the acidic site. Therefore, these results offer further support for the structure of CapC as deduced by NMR analysis (*vide supra*); in which, the structure is capable of the acid–base equilibrium depicted in Fig. 3.

Fluorescence properties of CapC were studied in acetonitrile solution. Acetonitrile was chosen in order to compare CapC's fluorescence properties with the previously reported *O*- and

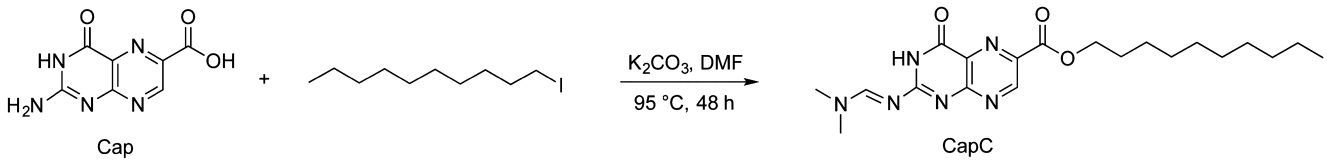

Scheme 1. Synthesis of CapC.

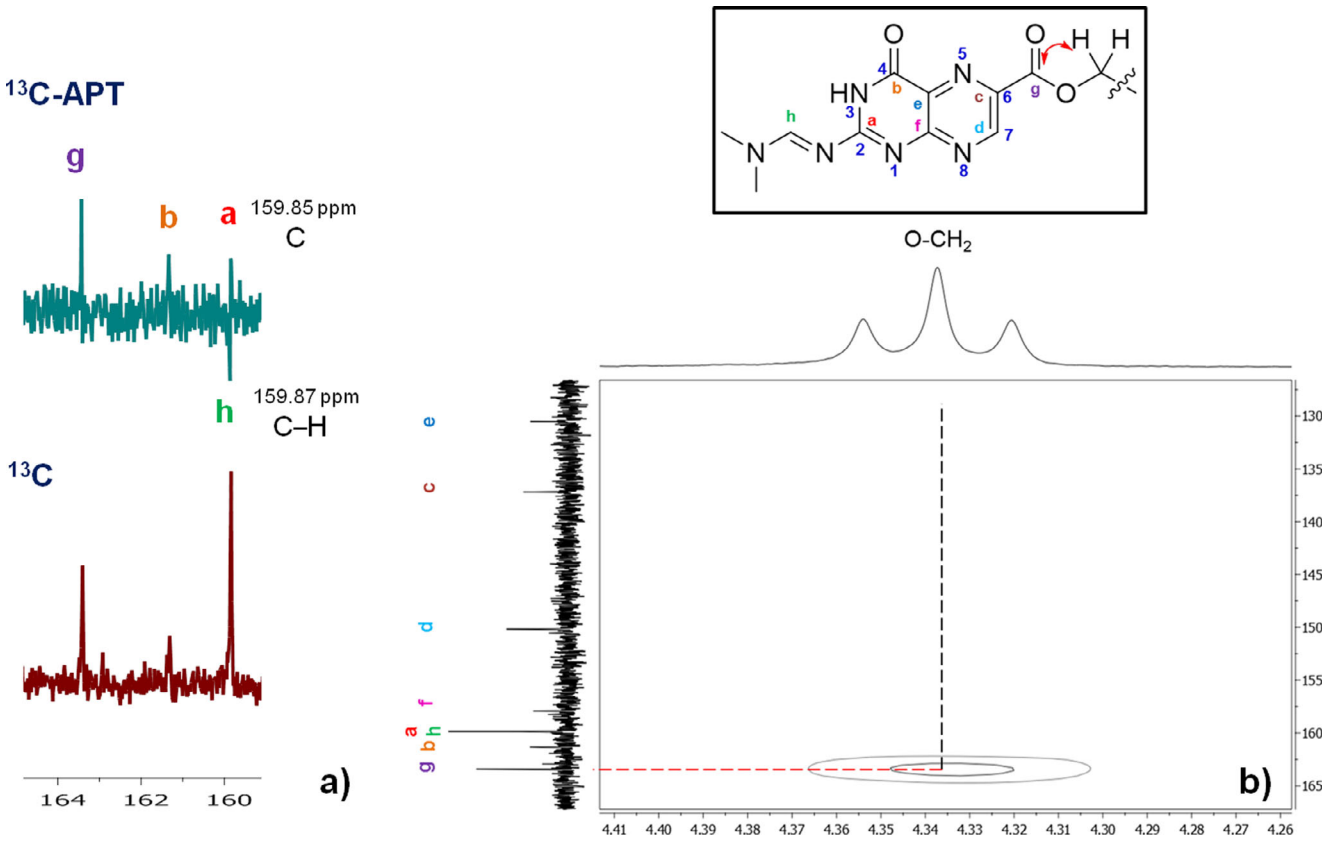

Figure 2. NMR spectra of CapC in DMSO-d_6: (a) expanded ^{13}C and ^{13}C-APT spectra showing two resolved peaks at 159.8 ppm and (b) expanded 2D HMBC spectrum shows a $^{3}J_{CH}$ correlation between O–CH_2 protons coupled to carbon "g" suggesting alkylation via carboxylic end.

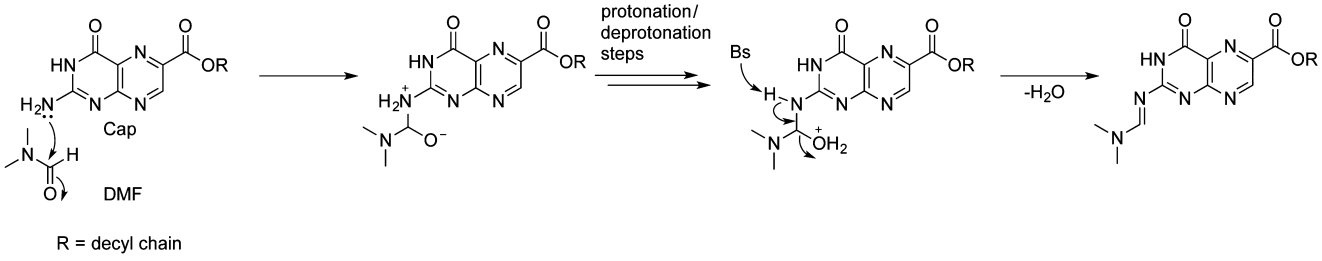

Scheme 2. Proposed mechanism of condensation of the DMF molecule onto the decylated Cap to form the biguanide-like segment of CapC.

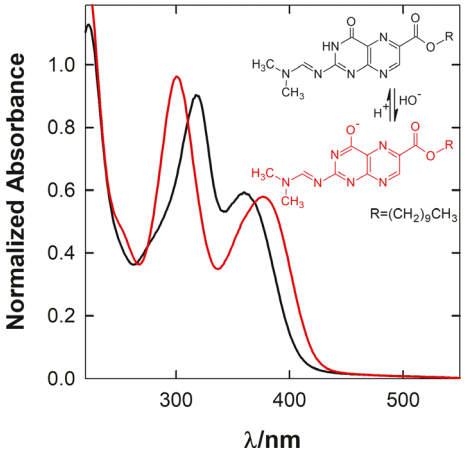

Figure 3. Absorption spectra of CapC in H_2O/methanol 3:1 (*v/v*) at pH 4 (black line) and at pH 11 (red line) and proposed acid–base equilibrium in protic solvents.

N-decyl-pterins **1**–**4**, also done in acetonitrile (10). CapC showed an absorption spectrum similar to the one previously observed for the acid form of CapC in methanol/water (Fig. 4) In addition, fluorescence emission data were collected. Excitation at 366 nm of CapC in acetonitrile showed an emission maximum at 428 nm. Furthermore, the fluorescence quantum yield (Φ_F) for CapC was determined to be 0.26 ± 0.02, which was nearly the same to the Φ_F previously reported for Cap in acidic media (0.28 ± 0.01) (3). Having the same Φ_F might be attributed to the fact that CapC has the chain attached to the substituent group and not directly to the ring, thereby not affecting the chromophore directly. In contrast, previously synthesized decyl-pterins **1**–**4**, which have the chain attached to the ring (10), have Φ_F an order of magnitude lower than CapC. Fluorescence emission was also study for CapC in methanol. Similar absorption and emission spectra were obtained compared to those in acetonitrile (see Supporting Information), although a redshift of 22 nm in the emission spectra of CapC was observed, with an emission

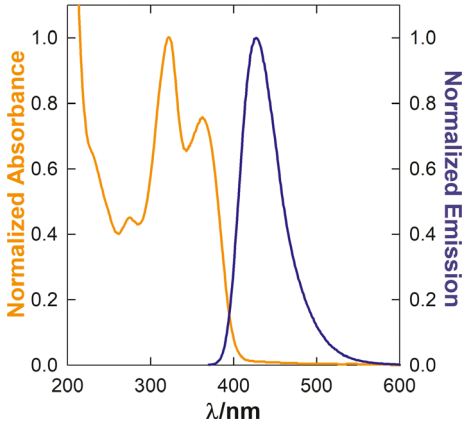

Figure 4. Normalized absorption (orange line) and emission (blue line) spectra of CapC in acetonitrile (λ_{exc} = 366 nm).

maximum at 449 nm. Moreover, Φ_F was determined as 0.19 ± 0.02, which was slightly lower than that observed in acetonitrile.

Next, the photosensitized $^1O_2$ production by CapC was investigated, using air-equilibrated acetonitrile solutions and monitoring its near-infrared luminescence at 1270 nm. Figure 5 shows the $^1O_2$ emission that was detected for CapC when exciting at 366 nm. The $^1O_2$ quantum yield (Φ_Δ) obtained was 0.40 ± 0.01, which is quite good and is similar to the Φ_Δ values reported for *O*- and *N*-decyl-pterins **1**–**4** (Φ_Δ = 0.35 to 0.50) (10).

Photochemical and thermal stability of CapC

The photo and thermal stability of CapC was examined in methanol and acetonitrile. Samples were kept in the dark at room temperature (25°C) and then injected in HPLC at different times. Results showed that CapC is stable with no detectable thermal degradation products in both solvents for at least 5 h. CapC displayed good photostability in methanol/water (50:50 v/v) when exposed to UVA radiation (see Materials and Methods). A low consumption of 6% of CapC was observed in 2 h of irradiation (see Supporting Information), in agreement with the high stability observed previously with DMF molecule-condensed pterins 2 and 4 (10).

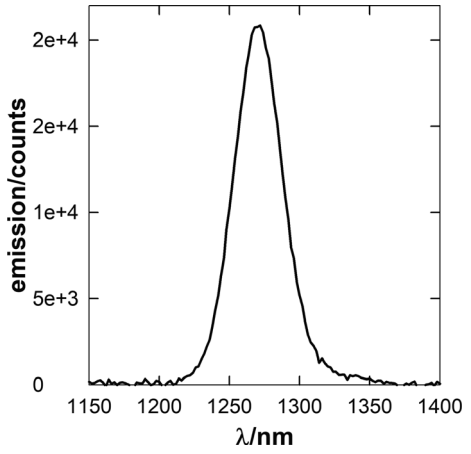

Figure 5. Singlet oxygen emission spectra of CapC in acetonitrile (λ_{exc} = 366 nm).

Computed solubility of CapC

The experimental and computational data showed that decyl-chain alkylation of Cap led to a significant increase in organic solvent solubility. CapC was found to have high solubility in organic solvents, such as DCM, DMSO, DMF and methanol. Solubility was also evaluated by calculating *P*, the partition coefficient of a neutral pterin (Fig. 6). Computed log *P* values, obtained with the ACD algorithm, were found to be −2.7 for Cap and 3.1 for CapC. The log *P* values of *O*-decyl-pterins **1** and **2** are found to be higher than CapC and the *N*-decyl-pterins **3** and **4**. Theoretical calculation of energetics of the pterin headgroup interaction with water compared to interaction within the membrane to deduce hydrogen bonding and van der Waals interactions, respectively, could provide insight in future work. The energetics of the former would be expected to be larger since a number of hydrogen bonds are likely between water molecules and the pterin heterocycle, especially in the case of ionizable protons positions in the amine and carboxylic acid groups in native pterin and Cap.

Membrane binding

To determine the binding constant (K_b) and therefore quantify the interaction of CapC with membranes (eggPC LUVs), titration curves at a constant concentration of compound and increasing concentration of lipid were carried out. The emission spectrum of the mixture corresponding to the maximum concentration of lipids used for the titration curve was monitored for up to 1 h and no significant changes were observed after 10 min of incubation, indicating that the system had reached the equilibrium. As a result, all measurements of the titration curves were performed after 15 min of incubation. As shown in Fig. 7, the binding constant of CapC to eggPC LUVs was obtained by fitting the fluorescence intensity as a function of the concentration of the LUVs and the value of K_b obtained was 8 (± 2) × 10^3 M^{-1}, which is in the same order of constants obtained for *O*- and *N*-decyl-pterins **1**–**4** (10) and other lipophilic compounds (38,39). The pterin moiety in CapC has the capacity to form hydrogen bonds with the water phase, even though native pterin is sparingly soluble in water itself. Thus, the chain extension of CapC will intercalate in the membrane, but the pterin headgroup may be situated at the water-membrane interface in a partial water interaction.

Interestingly, the Φ_F of CapC in LUVs was calculated at high concentration of lipid, where all compound intercalated in the membrane. The value obtained was 0.12 ± 0.05 which is higher than the one obtained in neutral water (0.017 ± 0.006). This increase in the fluorescence emission when CapC is intercalated signifies it to be an improved fluorescent probe in membranes.

SUMMARY

In summary, trifunctional uses for CapC have been found. CapC provides for simultaneous fluorescence detection, $^1O_2$ production and membrane localization. This is the first use of a pterin in a trimodal platform. As shown in Fig. 8, CapC is reasonably efficient in converting absorbed light into fluorescence emission with Φ_F of 0.26 in organic media and Φ_F of 0.12 in LUVs benefitting from its solubility and acid–base properties of the pterin headgroup. The fluorescence discrimination of CapC with a lower Φ_F of 0.017 in

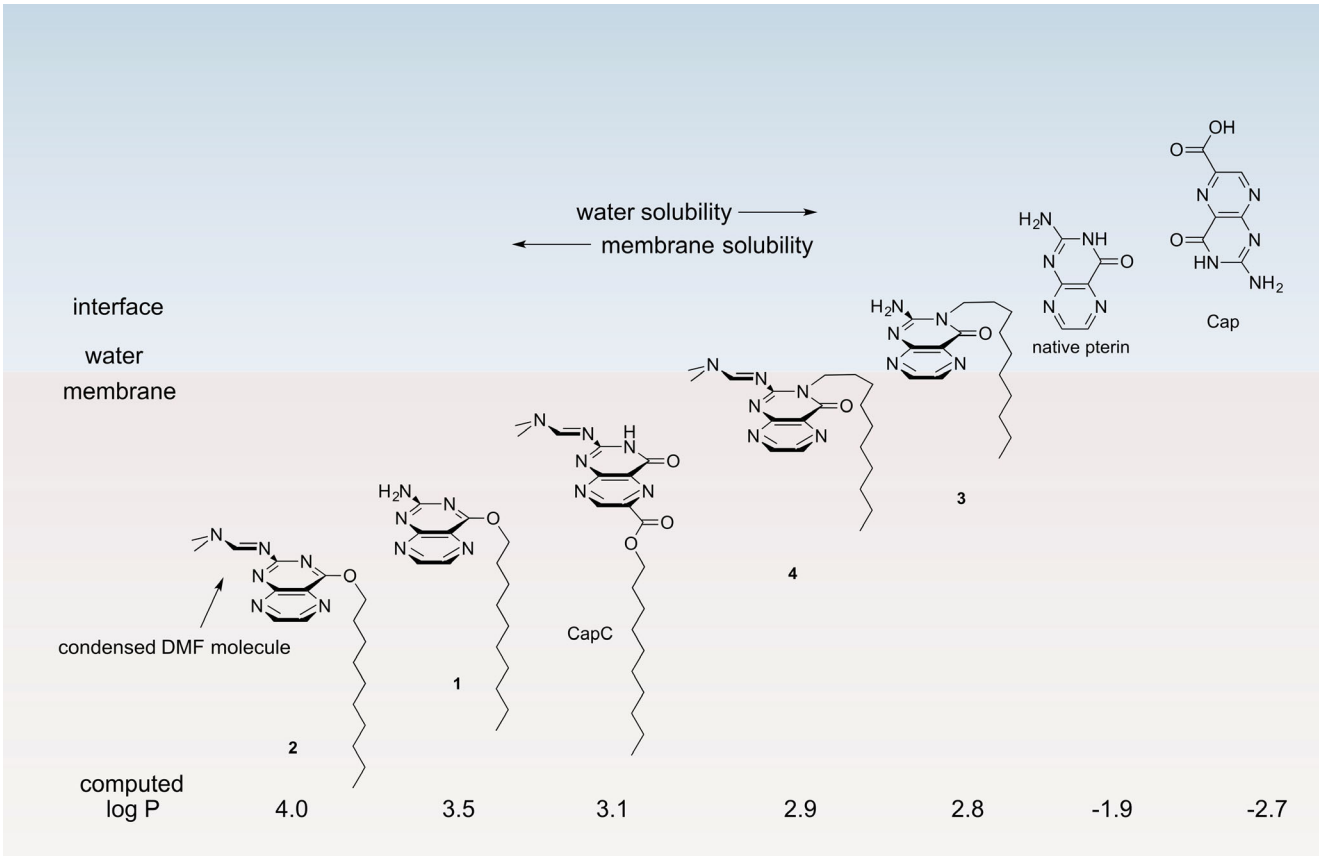

Figure 6. Proposed approximate interaction of pterin heads at or above the water/membrane interface. Computed log *P* data are also shown.

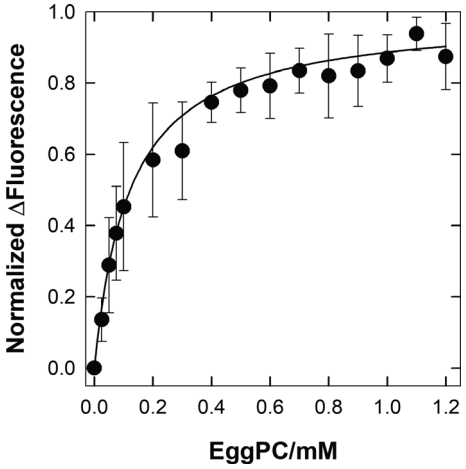

Figure 7. Association curves for CapC in eggPC LUVs.

water is sensible due to sparing solubility thereby making it more prone to aggregation. The previously reported Φ_F for Cap in acidic media is 0.28 (3), compared to the much lower levels of Φ_F for *O*- and *N*-decyl-pterins **1**–**4** with values between 0.01 and 0.08 in acetonitrile (10) where the structure integrity for the acid–base (keto–enol/enolate) equilibrium is lost. Concomitantly, CapC retains a favorable Φ_Δ of 0.40 in acetonitrile. This is a fairly good Φ_Δ and is comparable to quantum yields for *O*- and *N*-decyl-pterins **1**–**4** which ranged between 0.35 and 0.50, in acetonitrile (Table 1) (10). Membrane uptake of CapC was evident with a good binding constant K_b in LUV's of 8×10^3 M^{-1}, which is good and parallels to other membrane binders such as phthalocyanines (K_b = 1–7×10^3 M^{-1}) (40) and to some degree protoporphyrins bearing butyl and hexyl chains (K_b = 0.42 and 0.50 M^{-1}) (41).

The analysis of CapC's binding constant K_b and the Φ_F:Φ_Δ ratio of 0.26:0.40 results in a good triple function compound (Fig. 8). A higher quantum yield ratio is yet to be achieved. A Φ_F:Φ_Δ ratio approaching 0.4:0.6 was achieved by Arnaut *et al.* (42), even beyond net unity is theoretically possible, such as systems involving quantum chain reactions, as reported for photodecarbonylations by Garcia-Gariby *et al.* (43). Here, predictive tools would be useful, but are generally lacking, although correlations between computed close HOMO and LUMO energy levels (low HOMO-LUMO gaps), as well as the energy gap between S_1 and T_1 (44) and the use of Hammett constants (45), are important in designing fluorescent compounds and compounds prone to S-T intersystem crossing. Such information could provide predictive insight to design joint fluorescent and triplet sensitizer by structure–properties relationships of analogous compounds (46–48). Compounds and nanoparticles that can achieve high quantum yields of fluorescence and high $^1O_2$ quantum yields are of recent interest in image-guided PDT (49,50). Pterins have not yet been shown to be useful in this capacity in part due to their poor absorption of light in the visible and NIR. There is also wide interest in individual areas of highly emissive and amplified fluorescence materials (51–53), as well as sensitizers producing high yields of $^1O_2$ (38,54). In our case, inroads

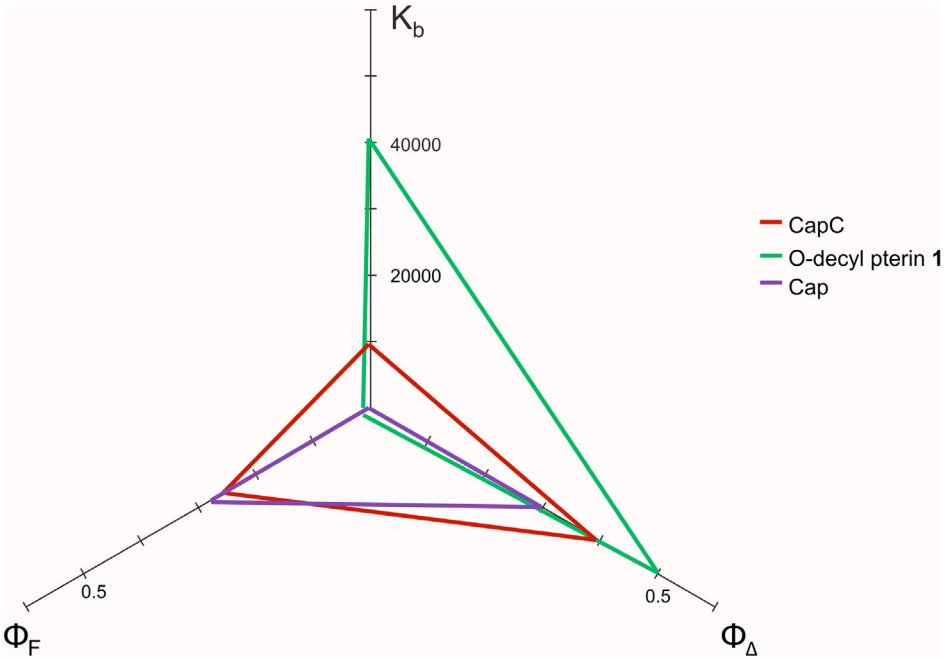

Figure 8. Plot comparing Cap, CapC, and *O*-decyl-pterin **1** binding constants (K_b) and quantum yields Φ_F and Φ_Δ.

Table 1. Fluorescence and singlet oxygen production quantum yields of pterin derivatives.

Compound	Fluorescence quantum yield $\Phi_F \pm$ SD	$^1O_2$ quantum yield $\Phi_\Delta \pm$ SD
Native pterin (basic form)*	0.27 ± 0.01	0.30 ± 0.02
Native pterin (acid form)*	0.33 ± 0.01	0.18 ± 0.02
Cap (basic form)*	0.18 ± 0.01	0.37 ± 0.02
Cap (acid form)*	0.28 ± 0.01	0.27 ± 0.03
CapC	0.26 ± 0.02	0.40 ± 0.01
1†	0.012 ± 0.002	0.50 ± 0.02
2†	0.078 ± 0.008	0.37 ± 0.02
3†	0.043 ± 0.005	0.36 ± 0.02
4†	0.076 ± 0.008	0.35 ± 0.01

*Data from Ref. 3. †Data from Ref. 10

have been made in the synthesis and characterization of CapC as a new lipophilic pterin in developing a self-monitoring fluorescent compound in the sensitized destruction effect upon delivery into the membrane.

CONCLUSION

In conclusion, we have synthesized and photochemically characterized CapC as a new lipophilic pterin that has the long alkane chain attached to the carboxyl group. We have considered how "distal" attachment of the alkane chain through the pendent carboxyl group provides easy access to a lipophilic pterin and leaves the pterin ring system less perturbed, which is unlike the previously reported *O*- and *N*-decyl-pterins **1–4** (10,11). Namely, the acid-base (keto–enol/enolate) equilibrium [N-C(=O)-NH ⇆ N-C(OH)=N ⇆ N-C(O^-)=N + H^+] of water-soluble (albeit sparingly water-soluble) portion of the pterin head is preserved in CapC. For the alkaline form of CapC, the absorption tail is slightly extended into the visible region. In contrast to *O*- or *N*-decyl-pterins, CapC contains a relatively good fluorescence emission and *also* retains triplet sensitization properties for a good quantum yield of $^1O_2$ production. Regarding lipophilicity, computed log *P* showed a value higher than Cap, and slightly lower than *N*-decyl-pterins, but slightly higher than the *O*-decyl-pterins perhaps due to a balance of the remotely connected decyl-chain and retention of the polar amide C=O and NH groups. However, the covalent bond of the long alkane chain through an ester in CapC is less stable to hydrolysis compared to the ether and amine sites in the *O*- and *N*-decyl-pterins **1–4**. Nonetheless, we show that the long alkane chain can be bound in CapC to efficiently intercalate in lipid membranes with a fairly high binding constant.

Finally, the generation and study of the new CapC will enable further efforts to combine lipophilic candidates for action both as a good fluorophore and $^1O_2$ sensitizer. The CapC structure will aid in the rational design of agents that can combine functions of a membrane fluorescent probe and a membrane photodamaging agent, to reveal pterin derivatives with more precise control over these functions. Thus far, the *O*- and *N*-decyl-pterins (10,11) and CapC relate to the alkyl chain locale, but are otherwise decyl-chain homologues. In the future, efforts could include generating pterins in screening techniques (e.g. high throughput screening) to better relate chain length and structural basis including even–odd carbon number effects causing membrane fluorescence *and* membrane photo-destruction.

Acknowledgements—This work was partially supported by Agencia Nacional de Promoción Científica y Tecnológica (ANPCyT-Grants PICT 2012-0508 and 2015-1988), Universidad Nacional de La Plata (UNLP-Grant X712). Authors thank Consejo Nacional de Investigaciones Científicas y Técnicas (CONICET) and National Science Foundation (NSF) for supporting their collaboration through a Bilateral Cooperation Programme Level I. M.N.U. thanks CONICET for a postdoctoral research fellowship. N.W. and A.G. thank the NSF for support (CHE-1464975). The authors gratefully acknowledge Nathalie Martins-Froment (Service Commun de Spectrométrie de Masse (FR2599), Université de

Toulouse III (Paul Sabatier)) for her contribution in mass spectrometry. M.V. and A.H.T. are research members of CONICET.

SUPPORTING INFORMATION

Additional supporting information may be found online in the Supporting Information section at the end of the article:

Figure S1. ^{1}H NMR of CapC in DMSO-d_6.

Figure S2. ^{13}C NMR of CapC in DMSO-d_6.

Figure S3. HMBC spectrum CapC in DMSO-d_6.

Figure S4. HRMS of CapC.

Figure S5. UV-Vis and Fluorescence spectra of CapC in methanol.

Figure S6. Time evolution of the absorption spectra of irradiated solution of CapC.

REFERENCES

1. Pfleiderer, W. (1993) Natural pteridines-a chemical hobby. In *Chemistry and Biology of Pteridines and Folates*, Vol. **338** (Edited by J. E. Ayling, M. Gopal Nair and C. M. Baugh), pp. 1–16. Plenum Press, New York.
2. Kappock, T. J. and J. P. Caradonna (1996) Pterin-dependent amino acid hydroxylases. *Chem. Rev.* **96**, 2659–2756.
3. Lorente, C. and A. H. Thomas (2006) Photophysics and photochemistry of pterins in aqueous solution. *Acc. Chem. Res.* **39**, 395–402.
4. Buglak, A. A., T. A. Telegina, E. A. Vorotelyak and A. I. Kononov (2019) Theoretical study of photoreactions between oxidized pterins and molecular oxygen. *J. Photochem. Photobiol., A* **372**, 254–259.
5. Baptista, M. S., J. Cadet, P. Di Mascio, A. A. Ghogare, A. Greer, M. R. Hamblin, C. Lorente, S. C. Nunez, M. S. Ribeiro, A. H. Thomas, M. Vignoni and T. M. Yoshimura (2017) Type I and II photosensitized oxidation reactions: guidelines and mechanistic pathways. *Photochem. Photobiol.* **93**, 912–919.
6. Estébanez, S., C. Lorente, M. G. Tosato, M. A. Miranda, M. L. Marín, V. Lhiaubet-Vallet and A. H. Thomas (2019) Photochemical formation of a fluorescent thymidine-pterin adduct in DNA. *Dyes Pigm.* **160**, 624–632.
7. Reid, L. O., E. A. Roman, A. H. Thomas and M. L. Dántola (2016) Photooxidation of tryptophan and tyrosine residues in human serum albumin sensitized by pterin: a model for globular protein photodamage in skin. *Biochemistry* **55**, 4777–4786.
8. Miñán, A., C. Lorente, A. Ipiña, A. H. Thomas, M. Fernández Lorenzo de Mele and P. L. Schilardi (2015) Photodynamic inactivation induced by carboxypterin: a novel non-toxic bactericidal strategy against planktonic cells and biofilms of staphylococcus aureus. *Biofouling* **31**, 459–468.
9. Thomas, A. H., Á. Catalá and M. Vignoni (2016) Soybean phosphatidylcholine liposomes as model membranes to study lipid peroxidation photoinduced by pterin. *Biochim. Biophys. Acta, Biomembr.* **1858**, 139–145.
10. Vignoni, M., N. Walalawela, S. M. Bonesi, A. Greer and A. H. Thomas (2018) Lipophilic decyl chain–pterin conjugates with sensitizer properties. *Mol. Pharm.* **15**, 798–807.
11. Walalawela, N., M. Vignoni, M. N. Urrutia, S. J. Belh, E. M. Greer, A. H. Thomas and A. Greer (2018) Kinetic control in the regioselective alkylation of pterin sensitizers: a synthetic, photochemical, and theoretical study. *Photochem. Photobiol.* **94**, 834–844.
12. Masuda, M., V. Vill and T. Shimizu (2000) Conformational and thermal phase behavior of oligomethylene chains constrained by carbohydrate hydrogen-bond networks. *J. Am. Chem. Soc.* **122**, 12327–12333.
13. Vignoni, M., M. N. Urrutia, H. C. Junqueira, A. Greer, A. Reis, M. S. Baptista, R. Itri and A. H. Thomas (2018) Photo-oxidation of unilamellar vesicles by a lipophilic pterin: deciphering biomembrane photodamage. *Langmuir* **34**, 15578–15586.
14. Huang, L., X. Cui, B. Therrien and J. Zhao (2013) Energy-funneling-based broadband visible-light-absorbing bodipy–C_{60} triads and tetrads as dual functional heavy-atom-free organic triplet photosensitizers for photocatalytic organic reactions. *Chem. Eur. J.* **19**, 17472–17482.
15. Yang, W., A. Karatay, J. Zhao, J. Song, L. Zhao, Y. Xing, C. Zhang, C. He, H. G. Yaglioglu, M. Hayvali, A. Elmali and B. Küçüköz (2015) Near-IR broadband-absorbing trans-bisphosphine Pt(II) bisacetylide complexes: preparation and study of the photophysics. *Inorg. Chem.* **54**, 7492–7505.
16. Frausto, F. and S. W. III Thomas (2018) Tuning the key properties of singlet oxygen-responsive acene-doped conjugated polymer nanoparticles. *ChemPhotoChem* **2**, 632–639.
17. van de Winckel, E., R. J. Schneider, A. de la Escosura and T. Torres (2015) Multifunctional logic in a photosensitizer with triple-mode fluorescent and photodynamic activity. *Chem. Eur. J.* **21**, 18551–18556.
18. Watley, R. L., S. G. Awuah, M. Bio, R. Cantu, H. B. Gobeze, V. N. Nesterov, S. K. Das, F. D'Souza and Y. You (2015) Dual functioning thieno-pyrrole fused bodipy dyes for nir optical imaging and photodynamic therapy: singlet oxygen generation without heavy halogen atom assistance. *Chem. Asian J.* **10**, 1335–1343.
19. Zhang, J., Y.-C. Liang, X. Lin, X. Zhu, L. Yan, S. Li, X. Yang, G. Zhu, A. L. Rogach, P. K. N. Yu, P. Shi, L.-C. Tu, C.-C. Chang, X. Zhang, X. Chen, W. Zhang and C.-S. Lee (2015) Self-monitoring and self-delivery of photosensitizer-doped nanoparticles for highly effective combination cancer therapy in vitro and in vivo. *ACS Nano* **9**, 9741–9756.
20. Patel, N., P. Pera, P. Joshi, M. Dukh, W. A. Tabaczynski, K. E. Siters, M. Kryman, R. R. Cheruku, F. Durrani, J. R. Missert, R. Watson, T. Y. Ohulchanskyy, E. C. Tracy, H. Baumann and R. K. Pandey (2016) Highly effective dual-function near-infrared (nir) photosensitizer for fluorescence imaging and photodynamic therapy (PDT) of cancer. *J. Med. Chem.* **59**, 9774–9787.
21. Hu, F., Y. Yuan, D. Mao, W. Wu and B. Liu (2017) Smart activatable and traceable dual-prodrug for image-guided combination photodynamic and chemo-therapy. *Biomaterials* **144**, 53–59.
22. Zhou, C., D. Afonso, S. Valetti, A. Feiler, V. Cardile, A. C. E. Graziano, S. Conoci and S. Sortino (2017) Targeted photodynamic therapy with a folate/sensitizer assembly produced from mesoporous silica. *Chem. Eur. J.* **23**, 7672–7676.
23. Chen, X., Y. Li, S. Li, M. Gao, L. Ren and B. Z. Tang (2018) Mitochondria- and lysosomes-targeted synergistic chemo-photodynamic therapy associated with self-monitoring by dual light-up fluorescence. *Adv. Funct. Mater.* **28**, 1804362.
24. Daniels, R. E., L. K. McKenzie, J. R. Shewring, J. A. Weinstein, V. N. Kozhevnikov and H. E. Bryant (2018) Pyridazine-bridged cationic diiridium complexes as potential dual-mode bioimaging probes. *RSC Advances* **8**, 9670–9676.
25. van de Winckel, E., M. Mascaraque, A. Zamarrón, Á. Juarranz de la Fuente, T. Torres and A. de la Escosura (2018) Dual role of subphthalocyanine dyes for optical imaging and therapy of cancer. *Adv. Funct. Mater.* **28**, 1705938.
26. Pollak, M. (2010) Metformin and other biguanides in oncology: advancing the research agenda. *Cancer Prev. Res. (Phila.)* **3**, 1060–1065.
27. Del Barco, S., A. Vazquez-Martin, S. Cufí, C. Oliveras-Ferraros, J. Bosch-Barrera, J. Joven, B. Martin-Castillo and J. A. Menendez (2011) Metformin: multi-faceted protection against cancer. *Oncotarget* **2**, 896–917.
28. Pollak, M. (2013) Potential applications for biguanides in oncology. *J. Clin. Invest.* **123**, 3693–3700.
29. Cerezo, M., T. Tomic, R. Ballotti and S. Rocchi (2015) Is it time to test biguanide metformin in the treatment of melanoma? *Pigm. Cell Melanoma R.* **28**, 8–20.
30. Dračínský, M. and R. Pohl (2014) Chapter 2: NMR studies of purines. In *Annual Reports on NMR Spectroscopy*, Vol. **82**. (Edited by G. A. Webb), pp. 59–113. Academic Press, Oxford, UK.
31. Serrano, M. P., M. Vignoni, M. L. Dántola, E. Oliveros, C. Lorente and A. H. Thomas (2011) Emission properties of dihydropterins in aqueous solutions. *Phys. Chem. Chem. Phys.* **13**, 7419–7425.
32. Eaton, D. F. (1988) Reference materials for fluorescence measurement. *Pure Appl. Chem.* **60**, 1107–1114.

33. Wilkinson, F., H. P. Helman and A. B. Ross (1995) Rate constants for the decay and reactions of the lowest electronically excited singlet state of molecular oxygen in solution. An expanded and revised compilation. *J. Phys. Chem. Ref. Data* **24**, 663–667.
34. Serrano, M. P., C. Lorente, C. D. Borsarelli and A. H. Thomas (2015) Unraveling the degradation mechanism of purine nucleotides photosensitized by pterins: the role of charge-transfer steps. *ChemPhysChem* **16**, 2244–2252.
35. Petrauskas, A. A. and E. A. Kolovanov (2000) ACD/Log P method description. *Perspect. Drug Discov.* **19**, 99–116.
36. Spessard, G. O. (1998) ACD Labs/LogP dB 3.5 and ChemSketch 3.5. *J. Chem. Inf. Comput. Sci.* **38**, 1250–1253.
37. Kuhn, H. J., S. E. Braslavsky and R. Schmidt (2004) Chemical actinometry (IUPAC Technical Report). *Pure Appl. Chem.* **76**, 2105–2146.
38. Angeli, N. G., M. G. Lagorio, E. A. S. Román and L. E. Dicelio (2000) *Meso*-substituted cationic porphyrins of biological interest. Photophysical and physicochemical properties in solution and bound to liposomes. *Photochem. Photobiol.* **72**, 49–56.
39. Calori, I. R., D. S. Pellosi, D. Vanzin, G. B. Cesar, P. C. S. Pereira, M. J. Politi, N. Hioka and W. Caetano (2016) Distribution of xanthene dyes in DPPC vesicles: Rationally accounting for drug partitioning using a membrane model. *J. Braz. Chem. Soc.* **27**, 1938–1948.
40. Calori, I. R. and A. C. Tedesco (2016) Lipid vesicles loading aluminum phthalocyanine chloride: formulation properties and disaggregation upon intracellular delivery. *J. Photochem. Photobiol., B* **160**, 240–247.
41. Bronshtein, I., M. Afri, H. Weitman, A. A. Frimer, K. M. Smith and B. Ehrenberg (2004) Porphyrin depth in lipid bilayers as determined by iodide and parallax fluorescence quenching methods and its effect on photosensitizing efficiency. *Biophys. J* . **87**, 1155–1164.
42. Silva, E. F., F. A. Schaberle, C. J. Monteiro, J. M. Dąbrowski and L. G. Arnaut (2013) The challenging combination of intense fluorescence and high singlet oxygen quantum yield in photostable chlorins–a contribution to theranostics. *Photochem. Photobiol. Sci.* **12**, 1187–1192.
43. Kuzmanich, G., M. N. Gard and M. A. Garcia-Garibay (2009) Photonic amplification by a singlet-state quantum chain reaction in the photodecarbonylation of crystalline diarylcyclopropenones. *J. Am. Chem. Soc.* **131**, 11606–11614.
44. Zilbershtein-Shklanovsky, L., M. Weitman, D. T. Major and B. Fischer (2013) Rules for the design of highly fluorescent nucleoside probes: 8-(substituted cinnamyl)-adenosine analogues. *J. Phys. Chem.* **78**, 11999–12008.
45. Greer, E. M. and K. Kwon (2018) Density functional theory and *ab initio* computational evidence for nitrosamine photoperoxides: Hammett substituent effects in the photogeneration of the nitrooxide intermediate. *Photochem. Photobiol.* **94**, 975–984.
46. Savarese, M., A. Aliberti, I. De Santo, E. Battista, F. Causa, P. A. Netti and N. Rega (2012) Fluorescence lifetimes and quantum yields of rhodamine derivatives: New insights from theory and experiment. *J. Phys. Chem. A* **116**, 7491–7497.
47. Fan, J., Y. Zhang, Y. Zhou, L. Lin and C.-K. Wang (2018) Excited state properties of a thermally activated delayed fluorescence molecule in solid phase studied by quantum mechanics/molecular mechanics method. *J. Phys. Chem. C* **122**, 2358–2366.
48. Lin, L., L. Cai, J. Fan and C.-K. Wang (2018) Electroluminescent mechanism of thermally activated delayed fluorescence emitters: Conformational effect. *J. Phys. Chem. C* **122**, 19953–19961.
49. Liu, X., M. Zheng, X. Kong, Y. Zhang, Q. Zeng, Z. Sun, W. Jan Buma and H. Zhang (2019) Separately doped upconversion-C_{60} nanoplatform for NIR imaging-guided photodynamic therapy of cancer cells. *Chem. Commun.* **49**, 3224–3226.
50. Zou, J., Z. Yin, P. Wang, D. Chen, J. Shao, Q. Zhang, L. Sun, W. Huang and X. Dong (2018) Photosensitizer synergistic effects: D–A–D structured organic molecule with enhanced fluorescence and singlet oxygen quantum yield for photodynamic therapy. *Chem. Sci.* **9**, 2188–2194.
51. Liu, H., Z. Wang, X. Wang, L. Shen, C. Zhang, M. Xiao and X. Li (2018) Singlet exciton fission in a linear tetracene tetramer. *J. Mater. Chem. C* **6**, 3245–3253.
52. Soper, S. A., H. L. Nutter, R. A. Keller, L. M. Davis and E. B. Shera (1993) The photophysical constants of several fluorescent dyes pertaining to ultrasensitive fluorescence spectroscopy. *Photochem. Photobiol.* **57**, 972–977.
53. Wang, Y., M. Zhi, Y.-Q. Chang, J.-P. Zhang and Y. Chan (2018) Stable, ultralow threshold amplified spontaneous emission from $CsPbBr_3$ nanoparticles exhibiting trion gain. *Nano Lett.* **18**, 4976–4984.
54. Liu, Y., R. Hammitt, D. A. Lutterman, L. E. Joyce, R. P. Thummel and C. Turro (2009) Ru(II) complexes of new tridentate ligands: Unexpected high yield of sensitized $^1O_2$. *Inorg. Chem.* **48**, 375–385.